MEMS Piezoresistive Sensor for Monitoring Bond Integrity in Adhesively Bonded Patches

H.H. Gharib, W.A. Moussa
University of Alberta, Edmonton, Canada

Abstract

The use of bonded patches in the repair of aircraft cracked structures has the advantage of reinforcing the cracked structure without inducing stress concentrations. However, one major limitation to the use of bonded patches in aircraft is the unavailability of a reliable monitoring technique that can monitor debonding of the adhesive bond due to adhesive degradation. This raises the need for a structural health monitoring (SHM) mechanism that can monitor the integrity of the adhesive bond in a repair patch.
In this paper, the design and simulation of an array of MEMS piezoresistive sensors for the detection of adhesive failure in bonded patches is presented. Piezoresistive sensors are used to measure the variation in strain at the patch-adhesive interface. A significant decrease in the measured strain is correlated to failure of the bond (debonding). The results of the finite element simulation are promising for the use of MEMS piezoresistors as a reliable SHM mechanism for detection of bond failure.

1   INTRODUCTION

The increase in the number of aging aircraft has raised the interest to develop reliable repair techniques for aircraft cracked structures. A common repair approach of cracked metallic structures is the use of repair patches, which are either riveted or bonded to the cracked structure. Compared to riveted patches, bonded repair patches offer the advantage of providing uniform load transfer from the cracked structure to the patch and reduced stress concentrations in the cracked structure. However, one limitation for the use of bonded patches is the fact that the adhesive bond deteriorates with time and consequently fails under operational loads. In order for bonded patches to be certified for use in military aircraft, it is required to have a reliable real-time means of evaluating the integrity of the adhesive bond. This raises the need for developing a smart patch that comprises a structural health monitoring (SHM) system capable of real-time assessment of the bond integrity and detecting the onset of debonding.

A great deal of research has been directed into developing monitoring techniques of patch debonding. Most of these efforts were focused on using optical fibers [1-3] or piezoelectric transducers [4-6]. These methods are successful in detecting the debonding of repair patches; however, they posses some weaknesses that delay their certification. These weaknesses are related to the use of conventional wiring and connectors to link the sensing elements to the outside world, which causes problems related to functionality, robustness, and severe electromagnetic

interference. Also, the harsh hydro-thermo-mechanical environment that affects aircraft raises many doubts about the reliability of such systems.

The need for an SHM system that meets the aircraft certification has raised the need for new and revolutionary sensing methods. Distributed MEMS sensors offer many advantages that make them a worthy option to explore. Compared to conventional methods, MEMS sensors are very much smaller, more robust, and consume much lower power. Also, MEMS sensors can be connected to other structural health monitoring elements using wireless communication which provide rapid communication and aid in solving airworthiness certification that is related to the wiring and connectors problem. Concerning fabrication cost, MEMS prototyping cost is high; however, once a final prototype is developed they can be microfabricated in mass-production quantities, which makes them potentially cheap.

Among the different MEMS sensors, piezoresistors are the most popular. The phenomenon of piezoresistivity is very interesting and useful in sensing stress, strain, or acceleration in a structure. Piezoresistive sensors can be used to detect debonding in bonded patches based on the load transfer criterion. This criterion is based on the fact that as long as the cracked structure is loaded, there is a strain transfer from the cracked structure to the composite patch through the adhesive. If the adhesive is debonded, this load transfer is broken and there will be a strain relief at the patch. Thus, an array of piezoresistors can be installed at the patch-adhesive interface to detect the onset of strain relief, which will be an indication of debonding. The use of the load transfer criterion in monitoring patch debonding has been used by other investigators [2, 3, 7]. However, most of these works are using macro sensing elements that are either surface mounted to the patch or embedded in the composite or adhesive bondline. This paper presents an SHM strategy for *in situ* monitoring of debonding of bonded repair patches using an embedded micro piezoresistive sensors array oriented along the patch-adhesive interface.

2   SENSING METHODOLOGY

2.1   Sensor array

Failure of adhesively bonded joints is mainly due to the increase in peel and out-of-plane shear stresses, which cause mode I and II cracks in the adhesive respectively [8]. For a bonded patch with uniaxial loading as shown in Figure 1, the maximum peel and shear stresses are located at the patch edge. Thus, debonding is expected to initiate from the patch edge and propagate towards the sheet crack line. Such phenomenon suggests that an effective sensing strategy is to arrange an array of sensors along the patch edge to capture the onset of debonding. The current study is proposing the use of an array of micro piezoresistive sensors arranged along the patch edges at the patch adhesive interface as shown in Figure 1.
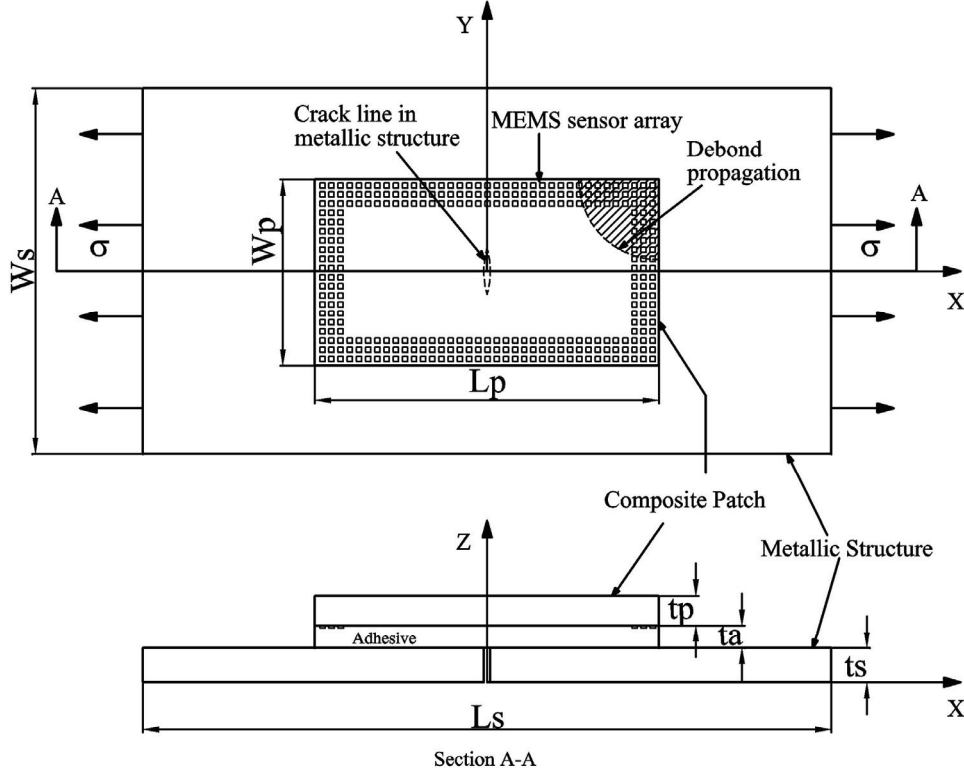
Y

Crack line in
metallic structure   MEMS sensor array

Debond
propagation

A   A

σ   σ

Ws   Wp

X

Lp

Composite Patch

Z

Metallic Structure

tp
ta
Adhesive
ts

Ls   X

Section A-A

Figure 1 Schematic of the bonded patch with sensor array

2.2 *Piezoresistive Sensor*

The proposed piezoresistive sensing mechanism will be able to evaluate four strain components while embedded in the adhesive bondline. According to Bittle et al [9], a piezoresistive sensor can be developed to measure four stress components (three normal stresses and one in-plane shear stress) through depositing p- and n-type piezoresistive elements on a (001) plane crystalline silicon wafer. This observation can be translated into a strain sensor that can measure the three normal and one in-plane shear strain components. Neglecting the effect of temperature on the change of resistance of a piezoresistive element, the equation for change in resistance as a function of strain components over the (001) plane is given by:

$$
\begin{aligned}
\frac{\Delta R}{R} = & \left[C_{12}\pi_{12} + C_{11}\left(\left(\frac{\pi_S - \pi_{44}}{2} \right) + \pi_{44}\cos^2\phi \right) + C_{12}\left(\left(\frac{\pi_S + \pi_{44}}{2} \right) - \pi_{44}\cos^2\phi \right) \right]\varepsilon_{xx} \\
& + \left[C_{12}\pi_{12} + C_{12}\left(\left(\frac{\pi_S - \pi_{44}}{2} \right) + \pi_{44}\cos^2\phi \right) + C_{11}\left(\left(\frac{\pi_S + \pi_{44}}{2} \right) - \pi_{44}\cos^2\phi \right) \right]\varepsilon_{yy} \\
& + \left[C_{11}\pi_{12} + C_{12}\pi_S \right]\varepsilon_{zz} + C_{44}\pi_D \sin(2\phi)\varepsilon_{xy}
\end{aligned}
\tag{1}
$$

3

Where,

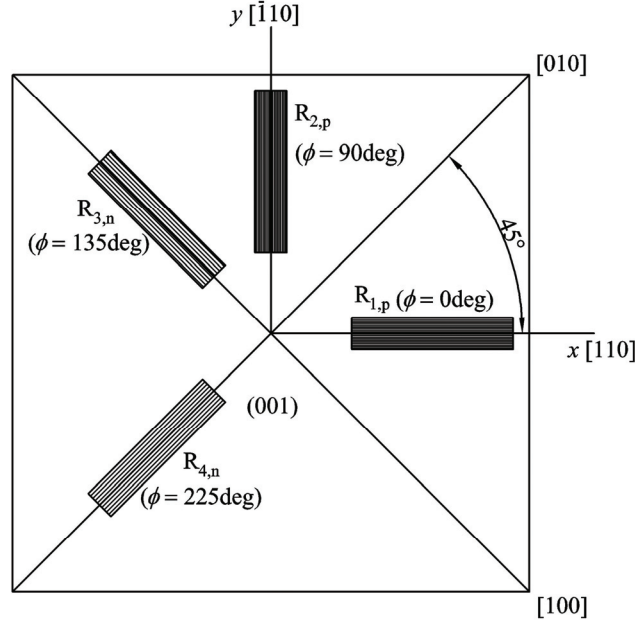ε_{ij} = strain components where i,j = x, y, z

C_{ij} = silicon stiffness components

π_{ij} = piezoresistive coefficients

π_S = $\pi_{11} - \pi_{12}$

π_D = $\pi_{11} + \pi_{12}$

ϕ = orientation angle of piezoresistive element over the (001) plane

Figure 2: Four element piezoresistive sensor

The four strain components given in Eq. (1) are evaluated by orienting four sensing elements over the (001) silicon plane. Two of these sensing elements are p-type doped at 0° and 90° orientation angle (ϕ) and two are n-type doped at 135° and 225° orientation angle (ϕ) as shown in Figure 2. Such arrangement gives the following four linear equations which can be solved simultaneously to evaluate ε_{xx}, ε_{yy}, ε_{zz} and ε_{xy} in the silicon wafer.

$$\frac{\Delta R_1}{R_1} = \left[C_{12} \left(\pi_{12}^p + \frac{\pi_S^p - \pi_{44}^p}{2} \right) + C_{11} \left(\frac{\pi_S^p + \pi_{44}^p}{2} \right) \right] \varepsilon_{xx} + \left[C_{12} \left(\pi_{12}^p + \frac{\pi_S^p + \pi_{44}^p}{2} \right) + C_{11} \left(\frac{\pi_S^p - \pi_{44}^p}{2} \right) \right] \varepsilon_{yy}$$

$$+ \left[C_{11} \pi_{12}^p + C_{12} \pi_S^p \right] \varepsilon_{zz} \tag{2}$$

$$\frac{\Delta R_2}{R_2} = \left[C_{12} \left(\pi_{12}^p + \frac{\pi_S^p + \pi_{44}^p}{2} \right) + C_{11} \left(\frac{\pi_S^p - \pi_{44}^p}{2} \right) \right] \varepsilon_{xx} + \left[C_{12} \left(\pi_{12}^p + \frac{\pi_S^p - \pi_{44}^p}{2} \right) + C_{11} \left(\frac{\pi_S^p + \pi_{44}^p}{2} \right) \right] \varepsilon_{yy}$$

$$+ \left[C_{11} \pi_{12}^p + C_{12} \pi_S^p \right] \varepsilon_{zz} \tag{3}$$

$$\frac{\Delta R_3}{R_3} = \left[C_{12}\left(\pi_{12}^n + \frac{\pi_S^n}{2} \right) + C_{11}\left(\frac{\pi_S^n}{2} \right) \right] \varepsilon_{xx} + \left[C_{12}\left(\pi_{12}^n + \frac{\pi_S^n}{2} \right) + C_{11}\left(\frac{\pi_S^n}{2} \right) \right] \varepsilon_{yy} + \left[C_{11}\pi_{12}^n + C_{12}\pi_S^n \right] \varepsilon_{zz}$$

$$-C_{44}\pi_D^n \varepsilon_{xy} \qquad\qquad (4)$$

$$\frac{\Delta R_4}{R_4} = \left[C_{12}\left(\pi_{12}^p + \frac{\pi_S^n}{2} \right) + C_{11}\left(\frac{\pi_S^n}{2} \right) \right] \varepsilon_{xx} + \left[C_{12}\left(\pi_{12}^n + \frac{\pi_S^n}{2} \right) + C_{11}\left(\frac{\pi_S^n}{2} \right) \right] \varepsilon_{yy} + \left[C_{11}\pi_{12}^n + C_{12}\pi_S^n \right] \varepsilon_{zz}$$

$$+C_{44}\pi_D^n \varepsilon_{xy} \qquad\qquad (5)$$

Where,

p and n superscripts designate p- and n-type doping.

3   ANALYSIS

The proposed sensing mechanism is simulated and analyzed using a developed finite element model. The modeled bonded patch is composed of an aluminum sheet, carbon fiber reinforced plastic (CFRP) patch, and FM-73 adhesive. The geometry and the material properties of the bonded patch components are given in Table 1. The simulated sensor array is made up of five sensors arranged along the patch edge in the y-direction at equal increments as shown in Figure 3. The selection of this distribution is due to the fact that debonding is expected to initiate along this edge [10]. The sensors are oriented such that the $x\text{-}y$ plane of the sensor shown in Figure 2 is coincident with the X-Y plane of the bonded patch shown in Figure 1. Each sensor is formed of four 100x20x2μm p- and n-type sensing elements deposited over a 1000x1000x30μm silicon wafer.

Table 1
Mechanical properties and geometry of the bonded patch

	Sheet - Aluminum	Patch - CFRP	Adhesive - FM73
E_x (GPa)	70	168	2.2
E_y, E_z (GPa)		10	
υ_{xy}, υ_{xz}	0.33	0.02	0.35
υ_{yz}		0.48	
G_{xy}, G_{xz} (GPa)		8	
G_{yz} (GPa)		4	
Length, L (mm)	300	150	150
Width, W (mm)	160	80	80
Thickness, t (mm)	3	1	0.2

Table 2
Piezoresistive coefficients and silicon stiffness components

Doping type	π_{11} (MPa^{-1})	π_{12} (MPa^{-1})	π_{44} (MPa^{-1})	C_{11} (GPa)	C_{12} (GPa)	C_{44} (GPa)
n-type	-102.2	53.4	-13.6	165.7	63.9	79.6
p-type	6.6	-1.1	138.1			

A coupled structural-piezoresistive finite element model is developed to simulate the output of the sensor array due to an applied load on the aluminum sheet. Only quarter model was analyzed due to the symmetry in the bonded patch geometry and loading. The model is developed using the commercial software ANSYS[®] 11 using SOLID186 10-noded tetrahedral element for the structural components and SOLID226 10-noded structural-piezoresistive coupled tetrahedral element for the piezoresistive sensing elements. The finite element mesh of one sensing element that is connected to a Wheatstone bridge configuration is shown in Figure 4. The nodes at the terminals of the sensing element are coupled in terms of voltage degree of freedom to obtain a uniform voltage value at the terminals. The piezoresistive coefficients and silicon stiffness components for the modeled sensors are given in Table 2. Due to the difference in scale between the sensor and the bonded patch structure, a fine mesh is created at the sensor locations and expands to a coarser mesh over the structural components.

Four cases were analyzed to simulate the effect of increasing the debond length on the sensor array output due to an applied axial load (σ) of 200MPa on the aluminum sheet along the positive x-direction. The four simulated cases are for a zero, 3mm, 6mm, and 9mm debond lengths as shown in Figure 3, where debonding is assumed to occur at the sheet-adhesive interface.
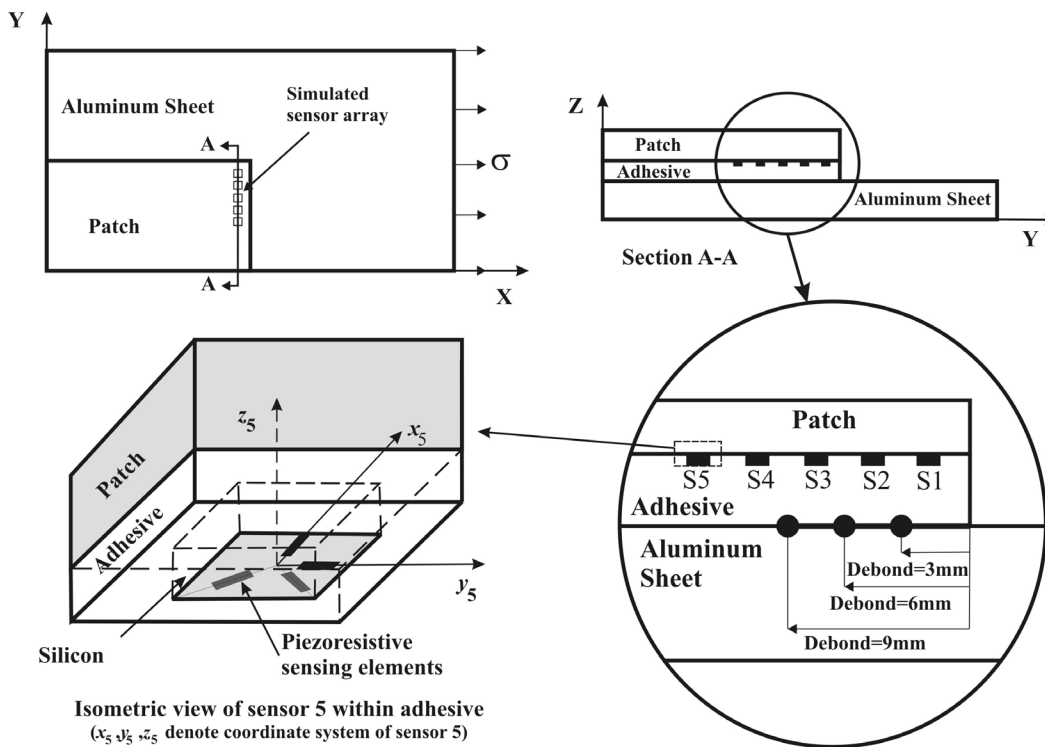

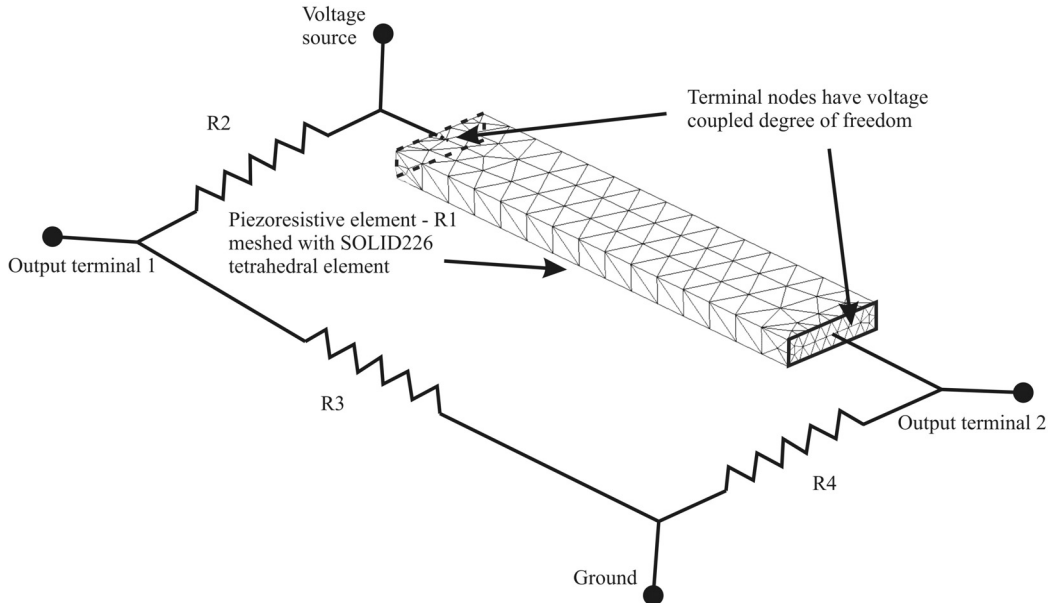**Figure 3 Schematic of the bonded patch finite element model**

Figure 4 Piezoresistive sensing element in a Wheatstone bridge configuration

4   RESULTS AND DISCUSSION

The output voltage from each sensing element is extracted from the finite element model and correlated to the change in resistance of the sensing element through Wheatstone bridge relations. The strain along the x-direction (ε_{11}) is evaluated from each sensor and for the four debond lengths cases based on the change in resistance of the four sensing elements.

A plot of ε_{11} from each sensor along the patch width is shown in Figure 5. Originally, when there is no debond, all sensors give almost the same strain value at around 0.82. When the debond length passes sensor S1 at 3mm from the patch edge, sensor S1 shows a drop in the strain value to around 0.04, while there is no change in the strain value from other sensors. The drop in the strain value from one sensor is expected to be a continuous function with respect to debond length. Thus, for a debond length of 1.5mm a strain value from sensor S1 is expected to be within the range of 0.82 and 0.04. As debond length increases to 6mm, it passes sensors S1 and S2 which show a sharp decrease in the strain value. The same occurs for a debond length of 9mm, where sensors S1, S2, and S3 show a drop in the strain value, while sensors S4 and S5 do not show significant change. From the shown results, it is apparent that as the debond length increases; a sharp decrease in the strain is apparent at the location of debond due to the drop in the load transfer. This variation in the strain distribution along the patch-adhesive interface can be correlated to the debonding of the patch.

7

The same approach of correlating the longitudinal strain to the patch edge can be applied to the general case of biaxial loading of the sheet. In this case, the sensor array will be distributed along the patch edge as discussed earlier in Figure 1. The output from the sensor array will give a contour plot of the strains ε_{11} and ε_{22} topography over the patch edge. A sudden drop of strain at any point over this contour will be an indication of debonding at this location. Also, it will be possible to trace the direction of debond propagation based on the known sensors positions. Thus, the proposed sensing mechanism is capable of detecting the occurrence of debonding of the patch, its location and propagation direction.
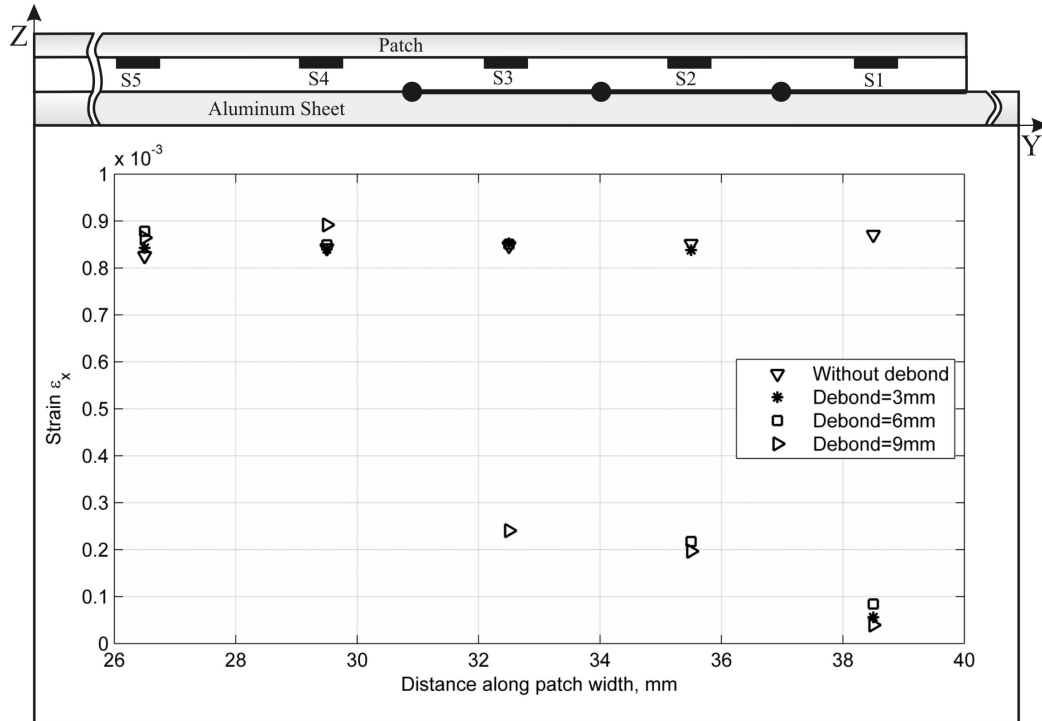

Figure 5 Strain output from the sensors along the patch width for different debond lengths

5 CONCLUSION

This paper presents a sensing mechanism based on the use of MEMS piezoresistive sensors for monitoring debonding of aircraft repair patches. The mechanism measures strain distribution over the patch edge to detect any discontinuity in the load transfer from the strained sheet to the patch. The sensors used in this mechanism are embedded along the patch-adhesive interface. Thus, they are affected by plane and normal loading conditions, which requires the use of a piezoresistive sensor that can take into account the effect of the normal strain component. This is resolved through using both p- and n-type doped piezoresistive elements.

A coupled structural-piezoresistive finite element model is developed to simulate the effect of debonding on the sensor array output. The results show that as debond length increases, the longitudinal strain component decreases. Therefore, debonding of the patch can be detected. The analysis can be extended to use a distributed sensor array over the patch edge which will give a contour plot of the strains topography over the patch edge. This approach would be able to detect the occurrence of debonding, its location, and propagation direction.

In this analysis, the effect of temperature on the change of resistance of the piezoresistive elements is neglected. Future studies are underway to include the effect of temperature, which will require different design of the piezoresistive sensing elements.

6   REFERENCES

[1] I. McKenzie, R. Jones, I.H. Marshall, S. Galea, Optical fibre sensors for health monitoring of bonded repair systems, Composite Structures 50 (4) (2000) 405-416
[2] J. Elster, A. Trego, J. Dante, M. Jones, J. Avram, Optical fiber-based adhesive bondline monitoring system for composite patch systems, Advanced Nondestructive Evaluation for Structural and Biological Health Monitoring 4335 188-195
[3] H.C.H. Li, F. Beck, O. Dupouy, I. Herszberg, P.R. Stoddart, C.E. Davis, A.P. Mouritz, Strain-based health assessment of bonded composite repairs, Composite Structures 76 (3) (2006) 234-242
[4] A.S. Islam, K.C. Craig, Damage detection in composite structures using piezoelectric materials, Smart Materials and Structures 3 (3) (1994) 318-328
[5] S.S. Kessler, S.M. Spearing, C. Soutis, Damage detection in composite materials using Lamb wave methods, Smart Materials & Structures 11 (2) (2002) 269-278
[6] A.R. Kumar, Dennis; Beard, Shawn; Qing, Xinlin; Hannum, Robert, In-situ monitoring of the integrity of bonded repair patches on aircraft and civil infrastructures, Advanced Sensor Technologies for Nondestructive Evaluation and Structural Health Monitoring II 6179 61790M
[7] R. Jones, S. Galea, Health monitoring of composite repairs and joints using optical fibres, Composite Structures 58 (3) (2002) 397-403
[8] L. Tong, G.P. Steven, Analysis and design of structural bonded joints, Kluwer Academic, Boston, Mass., (1999)
[9] D.A. Bittle, J.C. Suhling, R.E. Beaty, R.C. Jaeger, Piezoresistive stress sensors for structural analysis of electronic packages, Journal of Electronic Packaging 113 (3) (1991) 203-215
[10] P. Papanikos, K.I. Tserpes, S. Pantelakis, Initiation and progression of composite patch debonding in adhesively repaired cracked metallic sheets, Composite Structures 81 (2) (2007) 303-311